Bull. Univ. Osaka Pref., Ser. B, Vol. 41,
大阪府立大学紀要, 農学・生物学, 1989

Thermal Stress Analysis of Inspection Gallery Concrete

Satoru ISHIGURO

Laboratory of Land Development Engineering, College of Agriculture

(Received October 31, 1988)

Abstract

This paper describes the thermal stress properties of the culvert type inspection gallery, which is located on the rock foundation at the bottom of a fill dam. Thermal cracking of the inspection gallery concrete often occurs during construction. The cracking breaks water-tightness and durability of the inspection gallery. The tensile stress development in the concrete must be estimated to predict crack occurrence in the design.

In this study, the thermal behavior of the inspection gallery concrete during construction is discussed. The effects of a pipe-cooling, the restraints of the foundation rock, and the shapes of the cross section of the inspection gallery on the thermal stresses are also investigated by using finite element method. The results indicated that the maximum tensile stress developed in the cross section varies significantly with the degree of the restraint at the side surface. It was found that the pipe-cooling is a effective measure to reduce the thermal stresses in the concrete during construction.

Introduction

In recent years, the installation of an inspection gallery at the bottom of a fill dam has become standard to provide a space for grouting into foundations and to monitor dam behavior after construction. Inspection galleries installed in a fill dam are of two types, i.e., a culvert type and a tunnel type. This study deals with the culvert type inspection gallery.

The spacial dimensions of the inspection gallery and the temperature rise in the concrete during construction are both large enough to consider that the inspection gallery is one of mass concrete structures. Thermal cracking occurred in the structure is undersirable because it may break water-tightness and durability.

In addition, the cracks may reduce the safety of a fill dam. In the design, it is essential to predict the behavior of the thermal stresses during construction. The static stress behavior of the inspection gallery under embankment loads has been discussed in a previous report.[1)] This report describes the thermal stress properties of the inspection gallery during construction. The purposes of this study are as follows: to evaluate the effects of the pipe-cooling on the thermal stresses, to clarify the influences of the restraints of the foundation rock at the side surface on the thermal stresses, to investigate the influences of the shapes of the cross section on the thermal stresses.

Transient Temperature Analysis of the Inspection Gallery Concrete During Construction[2)]

Foundamental heat transfer equation for a two dimensional isotropic continuum is given by

$$\rho c\, \partial T/\partial t = k\,(\partial^2 T/\partial x^2 + \partial^2 T/\partial y^2) + Q \qquad (1)$$

where T: temperature (T(x, y, t)), ρ: unit volume weight, c: specific heat, k: thermal conductivity, Q: rate of heat generated

The thermal behavior in the concrete can be determined by solving the above equation. Boundary conditions such as fixed temperature boundary (S_1), heat flow boundary (S_2), and surface transfer boundary (S_3) must be taken into account in the analytical model. The boundary conditions can be specified mathematically as follows

$$T = \bar{T} \text{ on } S_1,\ q = q_0 \text{ on } S_2,\ q = \alpha\,(T - T_c) \text{ on } S_3 \qquad (2)$$

Where $q = -k\,(\partial T/\partial n)$, n: normal vector on boundary, α: coefficient of surface heat transfer, T_c: external temperature, $\bar{T}$: the value of fixed temperature, q_0: heat flux

Discretization of the differential equation by finite element method leads to the following matrix equation

$$[K]\,\{\phi\} + [C]\,\{\partial\phi/\partial t\} = \{F\} \qquad (3)$$

where [K] : heat conductivity matrix, [C] : heat capacity matrix, $\{F\}$: thermal flux vector, and $\{\phi\}$: vector of nodal temperature.

The iterative solution is summarized as follows. A small time increment Δt assumed is 6 hours.

a) At a time t, form [K], [C] and $\{F\}$. Calculate the rate of heat generated Q.
b) Modify [K] and $\{F\}$ to take the effect of the pipe-cooling[3)] into the analytical model.
c) Substituting [K], [C] and $\{F\}$ into Crank-Nicolson differential equation defined by

$$([K]/2 + [C]/\Delta t)\cdot\{\phi(t+\Delta t)\} = (-[K]/2 + [C]/\Delta t)\cdot\{\phi(t)\} + \{F\} \qquad (4)$$

in which, the temperature vector $\{\phi(t)\}$ in the right-hand side is known.

d) Solve the equation by Gaussian elimination method. Determine the temperature vector $\{\phi(t + \Delta t)\}$ at a time $t + \Delta t$.
e) The procedures from a) to d) are repeated with a small time increment Δt.

The location and the cross section of the inspection gallery in a fill dam are presented in Fig. 1. The inspection gallery is usually constructed at the two stages, i.e., a base concrete is placed at first, and a arch concrete is constructed after the base concrete has been hardened. The finite element idealization and the boundary conditions of the half cross section are shown in Fig. 2 and Fig. 3 respectively. Cooling pipes are embedded in the arch concrete. They are located at the nodal points of the finite element mesh. The pipe-cooling system works for 4 days after the placement of the arch concrete.

Material properties of the foundation rock, concrete, and cooling pipe are listed as

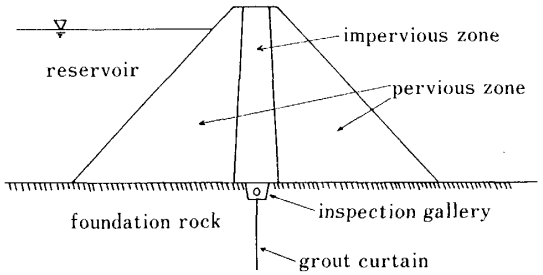

Fig. 1 Inspection gallery and its location in a fill dam

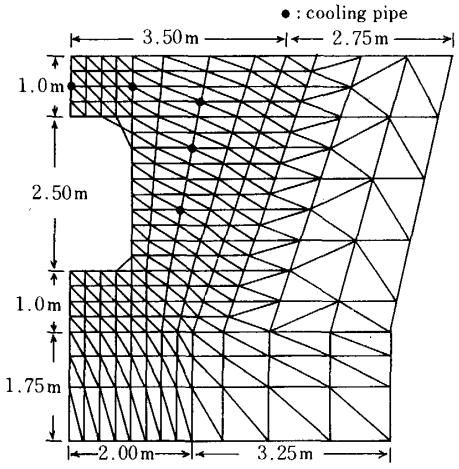

Fig. 2 Finite element idealization for temperature analysis (half cross section)

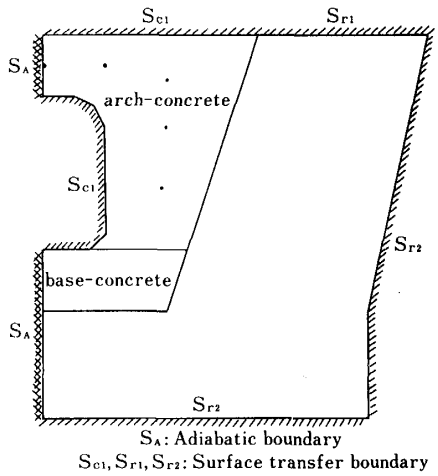

Fig. 3 Boundary conditions for temperature analysis

follows.

(1) Concrete

Unit volume weight ρ = 2300 kg/m^3, specific heat c = 0.23 kcal/°C, thermal conductivity k = 2.0 kcal/m·hr·°C, coefficient of surface heat transfer α_c = 10 kcal/m^2·hr·°C

Adiabatic temperature rise: $T_a = 40\,(1-e^{-0.8t})$

Rate of heat generated: $Q = \rho c \cdot dT_a/dt = 32\rho\, ce^{-0.8t}$

(2) foundation rock

Unit volume weight ρ = 2500 kg/m^3, specific heat c = 0.21 kcal/°C, thermal conductivity k = 1.5 kcal/m·hr·°C, coefficient of surface heat transfer α_{r1} = 7.5 kcal/m^2·hr·°C (at the upper surface); α_{r2} = 1.5 kcal/m^2·hr·°C (at the bottom and the outside surface)

(3) cooling pipe

Temperature of cooling water T_w = 10°C, diameter of cooling pipe D_p = 2.5 cm, coefficient of surface heat transfer between pipe and water α_p = 200 kcal/m^2·hr·°C

The thermal behavior of the concrete is traced for the period of 40 days from the start of the placement of the base concrete. The arch concrete is placed at 10 days later after the placement of the base concrete. Initial conditions for the transient temperature

analysis are assumed as follows.

Placement temperature of fresh concrete: 15°C
Atmospheric temperature: 10°C
Temperature of foundation rock: 10°C

Temperature changes at the sections of the arch crown and shoulder are represented in Fig. 4 and Fig. 5 respectively. In these figures, the temperature changes of the models with and without the pipe-cooling are compared. The maximum temperature rise of the no pipe-cooling model is about 20°C at the arch crown and is about 30°C at the shoulder. On the other hand, it is found that the temperature rise of the pipe-cooling model is depressed remarkably. The pipe-cooling lowers the concrete temperature only during cooling. The temperature rises again after the cooling has been stopped. After a maximum temperature has been reached, the temperature drops rapidly and finally equilibrates with the external temperature.

Analysis of Thermal Stress

The solution of the thermal stress problem[4] begins with the assumption that total change in strain during a time interval is the sum of the changes in elastic and thermal strain, i.e..

$$\{\Delta\epsilon\} = \{\Delta\epsilon^e\} + \{\Delta\epsilon^t\} \qquad (5)$$

where the superscripts e and t denote elastic and thermal strain respectively. The change in the elastic strains are thus

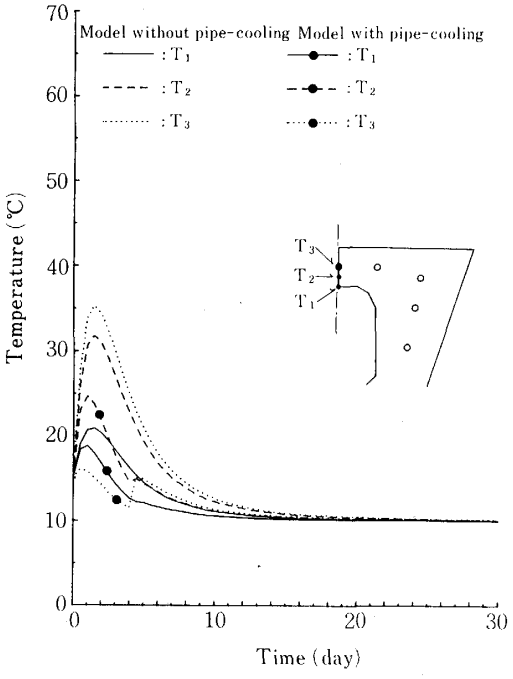

Fig. 4 Comparison of temperature variation curves with and without pipe-cooling in the arch crown

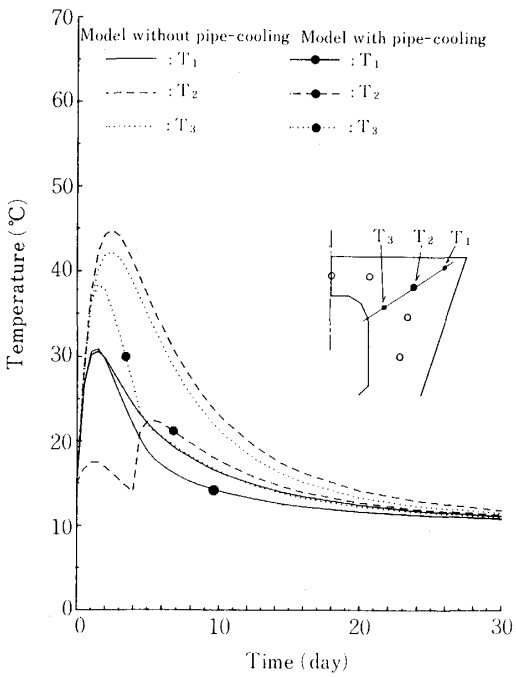

Fig. 5 Comparison of temperature variation curves with and without pipe-cooling in the shoulder

$$\{\Delta\epsilon^e\} = \{\Delta\epsilon\} - \{\Delta\epsilon^t\} \tag{6}$$

The incremental stresses are then related to the elastic strains by the general Hook's law equation

$$\{\Delta\sigma\} = [D^e]\ \{\Delta\epsilon^e\} \tag{7}$$

where $[D^e]$: elastic stress-strain matrix

Substituting eq.(5) into eq.(7) yields the relation between the incremental stress, total strain, and thermal strain

$$\{\Delta\sigma\} = [D^e]\ \{\{\Delta\epsilon\} - \{\Delta\epsilon^t\}\} \tag{8}$$

The other field equations are obtained from the relationship between strain and deformation. The incremental thermal strains subjected to the plane strain condition may be expressed as

$$\{\Delta\epsilon^t\} = \begin{Bmatrix} (1+\nu)\,\alpha\Delta t \\ (1+\nu)\,\alpha\Delta t \\ 0 \end{Bmatrix} \tag{9}$$

where α: thermal expansion coefficient, Δt: temperature change, ν: Poisson's ratio

Nodal forces equivalent to the thermal strains can be evaluated by

$$\{\Delta f_t\} = \int_{ve} [B]^T\ [D^e]\ \{\Delta\epsilon^t\}\ dv \tag{10}$$

where [B] : strain-displacement matrix, the superscript T denotes transpose matrix

The solution technique is summarized as follows:

a) At time t = 0, the elastic stresses are calculated.
b) Temperature changes during a small time increment Δt are determined from the results of the temperature analysis. And the incremental thermal strains are calculated from eq. (9).
c) The thermal strains are substituted into eq.(10) to evaluate the nodal forces equivalent to the thermal strains. The elastic deformation subjected to the nodal forces are analyzed and the incremental total strains $\{\Delta\epsilon\}$ are determined.
d) Finally, the incremental stresses are obtained from eq.(8) and are added to the previous stresses to yield the new stress distribution $\{\sigma_{t+\Delta t}\} = \{\sigma_t\} + \{\Delta\sigma\}$
e) The procedures from b) to d) are repeated with a small time increment Δt. Material properties such as Young's modulus and Poisson's ratio are assumed to remain constant during a small time increment.

The relations between the compressive strength and the age are assumed as shown in Fig. 6. The relationship can be expressed by the following equation

$$\sigma_c = \alpha \log_{10} M + \beta \tag{11}$$

where α and β are experimental constants respectively, M is the cumulative temperature defined by

$$M = \Sigma (10 + T) \cdot \Delta t \qquad (12)$$

where Δt: analytical time increment, T: concrete temperature during a time increment.

The Young's modulus and tensile strength of the concrete are respectively related to the compressive strength by the following equations

$$E_c = 40000 \cdot \sigma_c^{1/3} \quad (\mathrm{kgf/cm^2}) \qquad (13)$$

$$\sigma_t = 0.58 \cdot \sigma_c^{2/3} \quad (\mathrm{kgf/cm^2}) \qquad (14)$$

The Poisson's ratio is 0.167 and the thermal expansion coefficient is 10×10^{-6}.

The finite element model for the thermal stress analysis is represented in Fig. 7. Constant strain triangular elements are used in this model. The different boundary conditions which are shown in Fig. 8 are assumed to analyze the influences of the restraints on the thermal stresses. In Model 1, the vertical displacements of the joint between the base concrete and arch concrete are fixed. In Model 2, both the displacements of the joint and side surface are restrained completely.

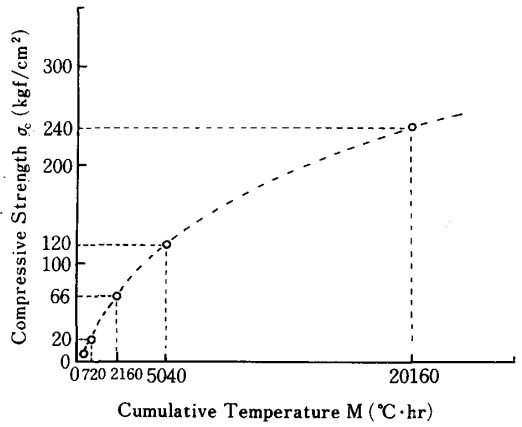

Fig. 6 Relations between compressive strength of concrete σ_c and cumulative temperature M

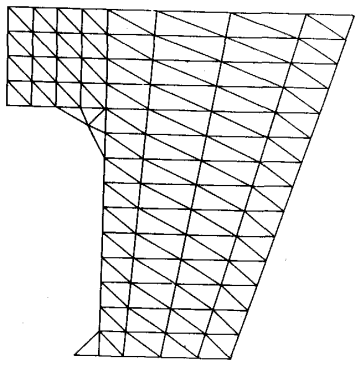

Fig. 7 Finite element model for thermal stress analysis

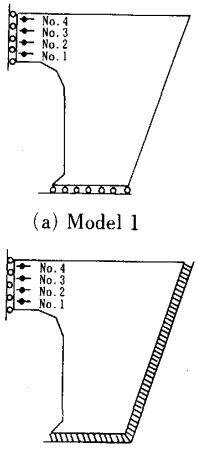

(a) Model 1

(b) Model 2

Fig. 8 Models with different boundary conditions

Behavior of Thermal Stress in Inspection Gallery

The thermal stress variations in the arch crown are shown in Fig. 9 and Fig. 10. The marks of No. 1 ~ No. 4 in these figures present the stresses of the horizontal direction. In each figure, comparisons are made on the thermal stress variation curves with and without the pipe-cooling. The results show that the thermal stresses of the pipe-cooling model are depressed remarkably compared with the no pipe-cooling model. The maximum tensile stress at the location No. 1 of Model 1 with the pipe-cooling is reached at the age 5 days. In this case, the concrete temperature of the section rises again after the cooling has been stopped, thus, the difference of the temperature between the inner part and surface becomes larger. In addition, the elastic modulus of the concrete at this age is about several times larger than that of the earlier age concrete. Consequently, the tensile stress induced is greater than that of the no pipe-cooling model.

The maximum principal stress distributions at the age 2 and 8 days are plotted in Fig. 11(a) and Fig. 11(b) respectively. From the results, it is found that tensile stresses develop at the locations such as the upper corner of the hole, the surface of the shoulder and the side surface. On the other hand, compressive stresses develop at the inside of the section. Fig. 11(e) presents the maximum principal stress distributions of the pipe-cooling model. It is noted that tensile stresses develop around the cooling pipes embedded.

The thermal stress behavior of Model 2 which is fixed at both the joint and side surface remarkably differs from the behavior of Model 1. During the temperature rise, restraining against the volumetric expansion causes compressive stress developments in the cross section. On the other hand, during the temperature drop, restraining against the contraction causes tensile stress developments. The maximum principal stress distributions of Model 2 are plotted in Fig. 11(c) and Fig. 11(d). The results indicate that tensile stresses develop at the surface of the hole at the age 2 days, and develop at the

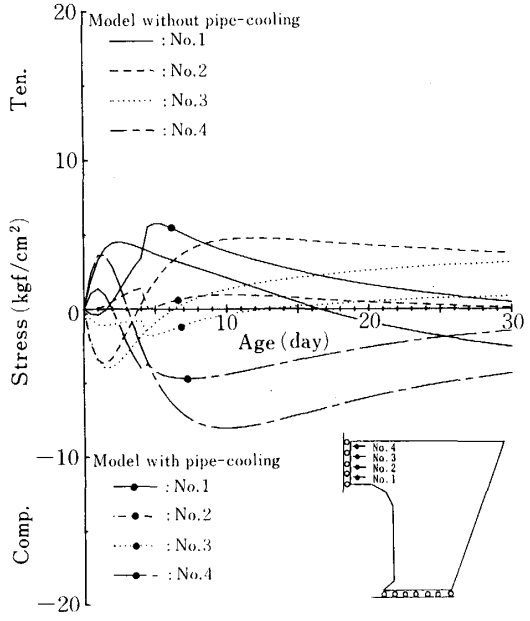

Fig. 9 Comparison of thermal stress variation curves with and without pipe-cooling (Model 1)

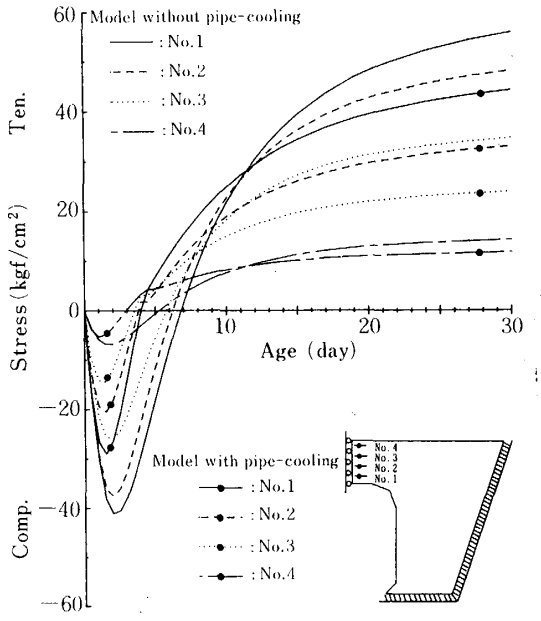

Fig. 10 Comparison of thermal stress variation curves with and without pipe-cooling (Model 2)

whole of the arch crown at the age 8 days.

Four models shown in Fig. 12 are analyzed to investigate the influences of the shapes on the thermal stresses. In Fig. 13, comparisons are made between Model A and Model B. The tensile stresses developed in the arch crown of Model B which is truncated at the corner of the shoulder are less than that of Model A. The results indicate that the restraint of the side surface gives a greater influence on the stresses of the arch crown.

In Fig. 14, comparisons are made between Model A and Model C to investigate the influences of the width of the section on the thermal stresses. The results show that the thermal stresses occurred in the arch crown decrease with shorting the width of the section. The rate of dissipation of the hydration heat in Model C is faster than that of Model A. Thus the maximum temperature rise is depressed. Consequently, the stresses in the arch crown of Model C change from compression to tension at earlier age than that of Model A.

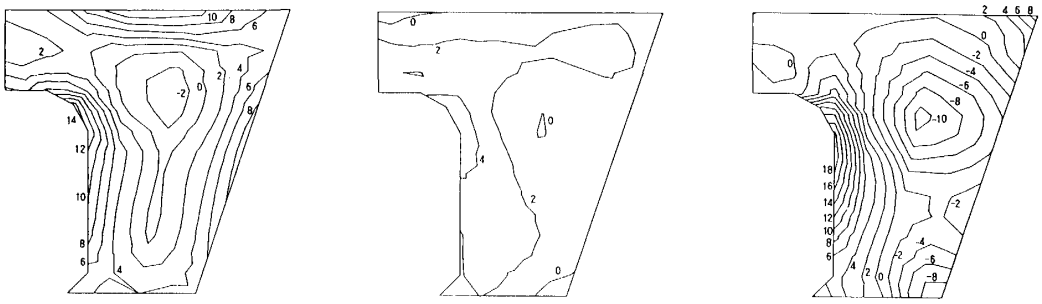

(a) Model 1 (age: 2 days) (b) Model 1 (age: 8 days) (c) Model 2 (age: 2 days)

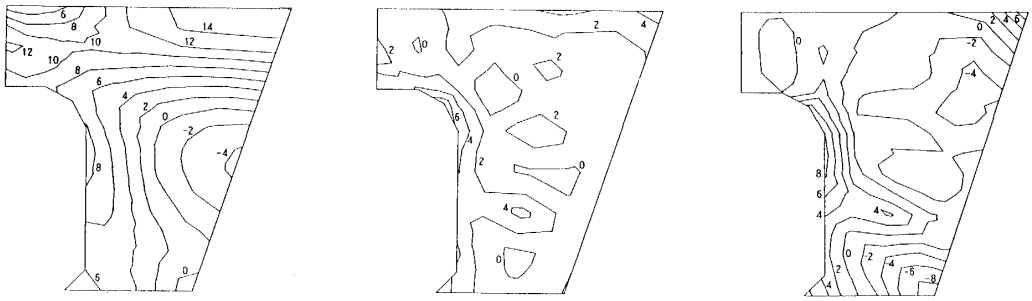

(d) Model 2 (age: 8 days) (e) Model 1 (age: 2 days, model with pipe-cooling) (f) Model 2 (age: 2 days, model with pipe-cooling)

Fig. 11 Contours of maximum principal stress in concrete (Unit: kgf/cm²)

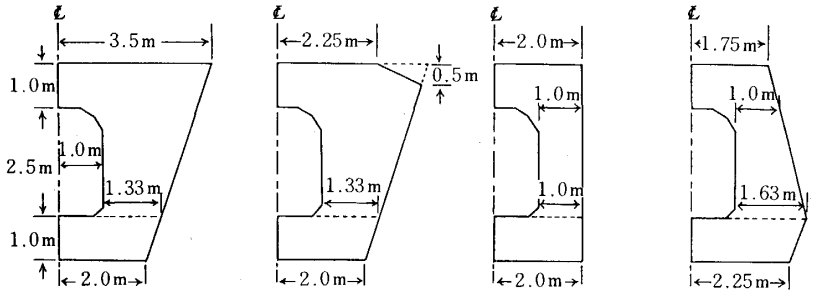

(a) Model A (b) Model B (c) Model C (d) Model D

Fig. 12 Half cross sections of culvert type inspection gallery

In Fig. 15, comparisons are made between Model C and Model D to determine the influences of the joint width on the thermal stresses. In this case, the side surface of the inspection gallery separates from the foundation rock. The results indicate that the thermal stresses induced in the arch crown increase with extending the width of the joint.

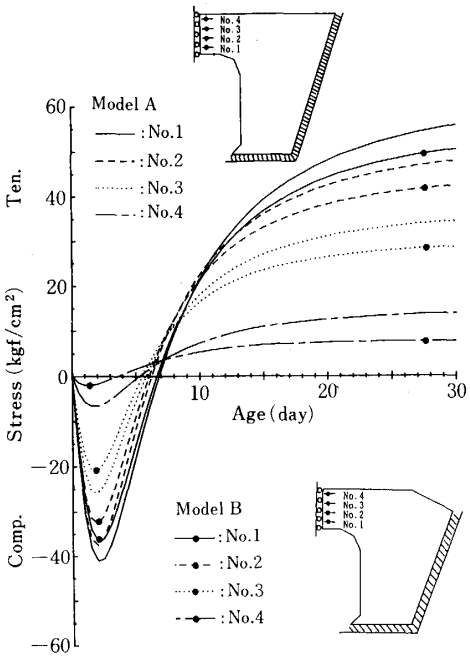

Fig. 13 Comparison of thermal stress variation curves between Model A and Model B

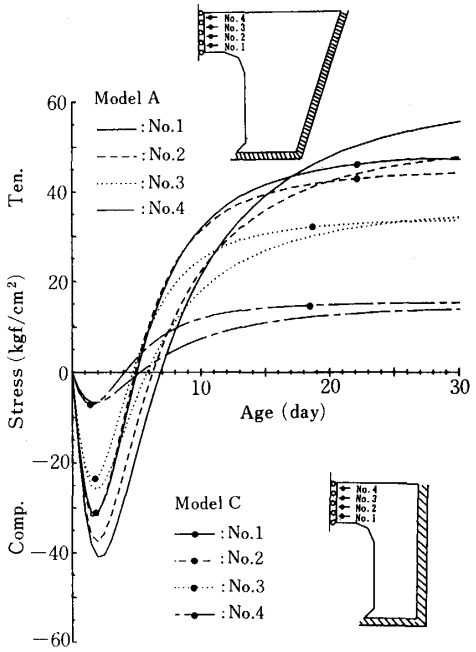

Fig. 14 Comparison of thermal stress variation curves between Model A and Model C

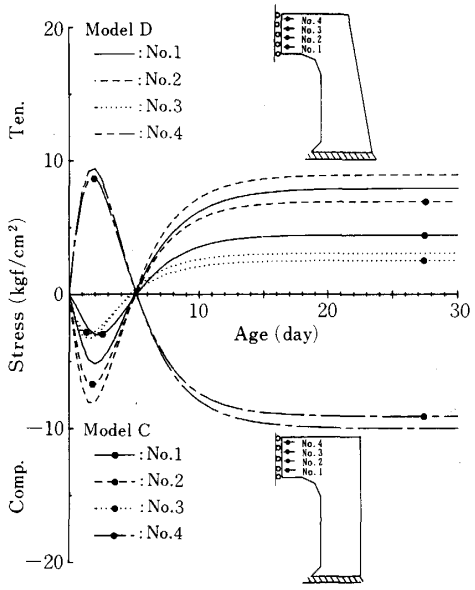

Fig. 15 Comparison of thermal stress Variation curves between Model C and Model D

Conclusions

In this paper, the thermal stress behavior of the inspection gallery concrete during construction are determined by using finite element method. From these results, the following conclusions are drawn.

(1) The restraints at the joint and side surface give a greater influence on the thermal stresses of the concrete. In order to prevent the occurrence of the thermal cracking during construction, the measures to reduce the restraints against the expansion and contraction of the concrete must be taken.

(2) The tensile stress developed in the arch crown may be controlled by varying the shapes such as the width of the section, the width of the joint and the corner of the shoulder.

(3) The pipe-cooling is a effective measure to depress the thermal stresses. However, it is noted that the tensile stress developed in the arch crown increases soon after the cooling has been stopped. Therefore, it should be avoided to stop the pipe-cooling too soon.

(4) Finite element method is a practical way to evaluate such properties as the transient heat transfer and the thermal stress variation in the inspection gallery concrete. The method also makes it possible to analyze the effect of the pipe-cooling.

References

1) ISHIGURO, S. and NAKAYA, M. (1984). Stress Analysis of Fill Dam Gallery. *Bull. Univ. Osaka Pref.*, **36**, 21–32.

2) ISHIGURO, S. and NAKAYA, M. (1986). Temperature Distribution Analysis of Concrete in Fill Dam Gallery. *Bull. Univ. Osaka Pref.*, **38**, 35–43.

3) WILSON, E.L. (1968). The Determination of Temperatures within Mass Concrete Structures. *Contract Report No. 68–17.* USAE Walla Dist., 16–18.

4) YAGAWA, G. and MIYAZAKI, N. (1985). *Netuōryoku·Kuripu·Netudendōkaiseki,* Saiensusha, 135–153 (*in Japanese*)